

Deconstructing the Catalytic Efficiency of Peroxiredoxin-5 Peroxidatic Cysteine

Stephanie Portillo-Ledesma,^{†,‡} Florencia Sardi,^{†,§} Bruno Manta,[§] María Victoria Tourn,[†] André Clippe,^{||} Bernard Knoops,^{||} Beatriz Alvarez,^{⊥,#} E. Laura Coitiño,[‡] and Gerardo Ferrer-Sueta^{*,†,#}

[†]Laboratorio de Físicoquímica Biológica, [‡]Laboratorio de Química Teórica y Computacional and [⊥]Laboratorio de Enzimología, Instituto de Química Biológica, Facultad de Ciencias, Universidad de la República, Montevideo, Uruguay

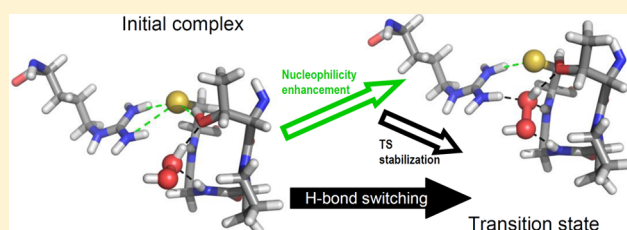
[§]Laboratory Redox Biology of Trypanosomes, Institut Pasteur de Montevideo, Montevideo, Uruguay

^{||}Laboratory of Cell Biology, Institut des Sciences de la Vie, Université Catholique de Louvain, B-1348 Louvain-la-Neuve, Belgium

[#]Center for Free Radical and Biomedical Research, Universidad de la República, Montevideo, Uruguay

S Supporting Information

ABSTRACT: Human peroxiredoxin-5 (PRDX5) is a thiol peroxidase that reduces H₂O₂ 10⁵ times faster than free cysteine. To assess the influence of two conserved residues on the reactivity of the critical cysteine (C47), we determined the reaction rate constants of PRDX5, wild type (WT), T44V and R127Q with one substrate electrophile (H₂O₂) and a nonspecific electrophile (monobromobimane). We also studied the corresponding reactions of low molecular weight (LMW) thiolates in order to construct a framework against which we could compare our proteins. To obtain a detailed analysis of the structural and energetic changes involved in the reaction between WT PRDX5 and H₂O₂, we performed ONIOM quantum mechanics/molecular mechanics (QM/MM) calculations with a QM region including 60 atoms of substrate and active site described by the B3LYP density functional and the 6-31+G(d,p) basis set; the rest of the protein was included in the MM region. Brønsted correlations reveal that the absence of T44 can increase the general nucleophilicity of the C47 but decreases the specific reactivity toward H₂O₂ by a factor of 10³. The R127Q mutation causes C47 to behave like a LMW thiolate in the two studied reactions. QM/MM results with WT PRDX5 showed that hydrogen bonds in the active site are the cornerstone of two effects that make catalysis possible: the enhancement of thiolate nucleophilicity upon substrate ingress and the stabilization of the transition state. In both effects, T44 has a central role. These effects occur in a precise temporal sequence that ensures that the selective nucleophilicity of C47 is available only for peroxide substrates.



Life evolved in the presence of H₂O₂, initially formed by water photolysis even before the advent of our oxygen atmosphere, in a process that still occurs today.¹ Evolution has produced a variety of enzymatic processes capable of managing and using H₂O₂ in controlled and beneficial ways. Among the enzymes related to H₂O₂ management, the thiol peroxidases known as peroxiredoxins appear as a successful strategy that has been conserved in all kingdoms of life.² Initially catalogued as antioxidant enzymes,³ it is increasingly evident that the reductive scavenging of hydroperoxides is only one of the possible functions of peroxiredoxins, along with oxidative folding⁴ and redox signaling.⁵

Peroxiredoxins are abundant, widespread, diverse, and apparently redundant in many biological compartments; their ability to reduce H₂O₂ arises from the striking reactivity of a conserved cysteine residue (the peroxidatic cysteine or C_P) toward hydroperoxides and peroxyacids in general. The reactivity of peroxiredoxins with H₂O₂, although remarkably high compared to other thiol proteins, has a broad range spanning 4 orders of magnitude in rate constants, from the

modest value for the bacterioferritin comigrating protein of *Escherichia coli* ($k_{app} = 9 \times 10^3 \text{ M}^{-1} \text{ s}^{-1}$ at room temperature and pH 7.4)⁶ to the near diffusion-controlled value for human peroxiredoxin 2 (PRDX2, $k_{app} = 10^8 \text{ M}^{-1} \text{ s}^{-1}$ at 25 °C and pH 7.4).⁷ Additionally, different peroxiredoxins possess different substrate preferences for H₂O₂,⁷ ONOOH,⁸ or lipid hydroperoxides,⁹ and they react poorly with non-peroxidic electrophiles.¹⁰ Neither the difference in reactivity toward a single hydroperoxide nor the substrate specificity among different peroxides is yet fully understood.

An important subgroup of peroxiredoxins is known as 2-Cys Prx as they use two cysteine residues in a catalytic cycle composed by three reactions in sequence.¹¹ Briefly, the C_P of the enzyme reacts with H₂O₂ forming a sulfenic acid and water. A second cysteine (the resolving cysteine or C_R) then condenses with the C_P sulfenic to form a disulfide and a

Received: March 30, 2014

Revised: September 1, 2014

Published: September 3, 2014

second water molecule. Finally, the disulfide is reduced, usually by a thioredoxin, in a series of two thiol–disulfide exchange reactions. Within 2-Cys Prx, human peroxiredoxin-5 (PRDX5) constitutes a very convenient system for studying the reactivity of these thiol peroxidases. From a structural standpoint, PRDX5 is one of the best-characterized peroxiredoxins. To date, it has eight entries in the protein data bank covering reduced (PDB ID: 1HD2, 1H4O, 1OC3, 2VL2, 3MNG), oxidized (PDB ID: 2VL3, 2VL9), and active-site mutants (PDB ID: 1URM); several bound to different ligands, all of which have helped shed light on the binding of substrate and its general reaction mechanism.^{12–15} The functional unit of PRDX5 is a 17 kDa monomer, a feature that makes the use of computational chemistry methods well suited to model its reactions in detail. The single tryptophan residue serves as a very convenient reporter of the redox state of the C_p, changing its fluorescent emission from reduced to sulfenic and to disulfide.⁸ As the vast majority of peroxiredoxins, the active site of reduced PRDX5 contains the C_p (C47) occupying the bottom of a deep and narrow pit, surrounded by three conserved residues, P40, T44, and R127.¹¹ In addition to the structural characteristics, the kinetics and mechanism of peroxide reduction have been studied, and some insight into the mechanisms has been gained.^{8,16}

The binding of remote groups of the substrate to specific sites in the enzyme, that is often invoked to account for enzymatic catalysis and specificity,¹⁷ cannot be applied in the case of H₂O₂ owing to its tiny size. In the absence of transition metal catalysis, the most important molecular interactions of H₂O₂ with its specific enzymes are hydrogen bonds (HB). This possibility has been explored several times in the past; for instance, on the grounds of an extensive survey of reported structures, Hall et al.¹⁴ have proposed that the positioning of H₂O₂ in the active site of peroxiredoxins would occur via a network of HB involving R127 and the amide groups of C47 and G46 as donors and T44 as acceptor (PRDX5 numbering). This HB network defines two oxygen-binding sites in an “oxygen-track”, which aligns the peroxide bond with the C_p thiolate in a nearly ideal geometry for the nucleophilic attack. Additional to H₂O₂ binding, the analysis of structures led to the proposal of a stabilization of the transition state (TS) of the reaction. Being an S_N2 reaction involving an anionic nucleophile and a neutral electrophile, the TS is expected to be linear and negatively charged; thus the positive charge of R127 and the weak interactions in the oxygen track from the amide groups of C47 and G46, and alcohol of T44 would provide the TS stabilization needed to account for the rate enhancement.

Whereas the activation of the thiolate of C47 as a nucleophile has also been proposed as a cause of the enhanced reactivity toward H₂O₂,¹⁴ this is not evident from the available structural data. In fact, most authors consider that the thiolate is stabilized by the electrostatic and HB interactions with the neighboring residues. Stabilization would actually oppose nucleophilicity, as is the case of LMW thiolates which are quite slow in their reaction with H₂O₂ in aqueous solution, with apparent rate constants <10 M⁻¹ s⁻¹ at pH 7.4 and 37 °C.¹⁸ This poor reactivity can be explained in part by the strong anion-solvating power and hydrogen-bonding ability of water that very effectively stabilizes thiolates. It has been shown that polar aprotic solvents such as dimethyl sulfoxide enhance the nucleophilicity of thiolates relative to aqueous solution¹⁹ and

that a single HB can decrease the rate constant of an alkylation reaction by 2 orders of magnitude.²⁰

As mentioned above, the stabilizing network of C47 thiolate involves the conserved residues T44 and R127. The alcohol group of T44 is well placed to form a HB with the thiolate ($d_{O-S} = 3 \text{ \AA}$),²¹ which could limit the nucleophilicity of the sulfur. The involvement of R127 is more complex; it could also act as a hydrogen-bond donor through its guanidinium group ($d_{N-S} = 3.3$ and 3.7 \AA), but the main interaction seems to be a salt bridge responsible for the stability of the thiolate, and probably for maintaining the architecture of the active site.

We previously proposed that the HB and weak interactions of the C47 could be used by the enzyme to enhance its specific reactivity if those interactions were switched off upon substrate binding;²² the consequent destabilization of the thiolate would then promote its nucleophilic attack on the bound hydroperoxide. Accordingly, we proposed that removing T44 or R127, the residues responsible for the stabilization of the thiolate, would allow the assessment of their influence on the nucleophilicity of C47.

The role of protons in the catalytic mechanism of peroxiredoxins has been extensively discussed, starting from the extreme importance initially attributed to the low pK_a of the C_p, to the fact that, the leaving group being a strong base, the rate of reaction could be hypothetically enhanced by partial proton donation to H₂O₂.²³ We have discussed previously that the acidic nature of the C_p can be regarded as a side effect of an active site selected to specifically bind an anionic transition state.²² Thiolates (and not thiols) are the reacting species and PRDXs have acidic pK_a's relative to what is expected for an ordinary peptidic cysteine. The low pK_a determines that most of the cysteine is ionized and thus available for catalysis at neutral pH. However, the pK_a of protein cysteines does not correlate to their specific reactivity; as a matter of fact, many other proteins possess pK_a's similar or even lower than PRDXs but lack any special reactivity toward H₂O₂.²⁴ Thus, the pK_a of a protein cysteine cannot be used as a predictor of its reactivity. Protonation of the peroxide substrate or the transition state to provide a better leaving group is a very appealing idea.¹¹ In the case of H₂O₂, protonation would produce dioxidanium (H₃O₂⁺), which is indeed a much better electrophile.²⁵ Both experimental and theoretical studies conducted in the gas phase provide evidence to sustain that protonation activates the species for unimolecular and S_N2 reactions involving O–O dissociation.^{25,26} However, H₃O₂⁺ is extremely acidic and only stable in superacid media.²⁷ Therefore, proton donation from R127, or any other acid in the active site of PRDX5, would be extremely unfavorable.

In this article, we intend to contribute to the understanding of the different components of the reactivity of C_p in PRDX5 by probing it from several directions. To better understand the nucleophilicity of the thiolate, we have measured the rate constant of C47 toward monobromobimane (mBr), a nonspecific electrophile. We studied the reaction of the wild type (WT) enzyme and of T44V and R127Q mutants. These rate constants were compared to those of LMW thiolates, also determined herein, which were used as a framework to interpret the rate constants in terms of general nucleophilicity. In order to gain further understanding on the influence of those active-site residues on the specific reaction of the enzyme, we also studied the reaction kinetics of H₂O₂ with WT, T44V, and R127Q mutant proteins, also in comparison with the rate constants of LMW thiolates. Finally, the reaction of WT

PRDX5 with H₂O₂ was modeled using ONIOM hybrid quantum mechanics/molecular mechanics (QM/MM) methods to obtain a detailed analysis of the structural and energetic changes involved in the reaction, paying particular attention to the evolution of the features of the HB network in the active site.

EXPERIMENTAL AND COMPUTATIONAL PROCEDURES

Chemicals. L-Cysteine hydrochloride monohydrate (Amresco), L-cysteine ethyl ester, 2-mercaptoethanol (Aldrich), 1-[2(S)-3-mercapto-2-methyl-1-oxopropyl]-L-proline (captopril), glutathione (GSH), L-cysteinyl-glycine, N-acetyl-L-cysteine (NAC), and meso-2,3-dimercaptosuccinic acid (DMSA) (Sigma) were used without further purification. Homocysteine was prepared from DL-homocysteine thiolactone (Sigma) by incubation with 5 M NaOH for 5 min at 37 °C followed by neutralization with 5 M HCl to pH < 2.

Thiol concentration was determined by chromogenic disulfide reduction using 4,4'-dithiodipyridine (Acros), $\epsilon_{324} = 21400 \text{ M}^{-1} \text{ cm}^{-1}$.²⁸ PRDX5 concentration was measured by absorbance at 280 nm ($\epsilon = 5500 \text{ M}^{-1} \text{ cm}^{-1}$).²⁹ Monobromobimane (either Sigma or Life Technologies) was dissolved in acetonitrile to prepare stock solutions (10–20 mM) that were stored in the dark at –20 °C. These solutions are stable for several months and were periodically quantified by the absorbance of a freshly prepared water-diluted sample ($\epsilon_{396} = 5300 \text{ M}^{-1} \text{ cm}^{-1}$).³⁰ Hydrogen peroxide solutions were prepared by diluting a stock solution of 30% H₂O₂ (Baker) and quantitated by their absorbance in the UV ($\epsilon_{240} = 43.6 \text{ M}^{-1} \text{ cm}^{-1}$).³¹

Buffer Systems. Unless otherwise specified, we have used wide-range buffer solutions of constant ionic strength ($I = 0.15$) independent of the pH. To that end, two of the mixtures proposed by Ellis³² were employed: the tris-MES-acetic buffer, consisting of 30 mM tris (Applichem) plus 15 mM MES (Applichem) plus 15 mM acetic acid (Dorwil) in the pH range of 3.5 to 9.0 or the ethanolamine-tris-ACES buffer, consisting of 15.6 mM ethanolamine (Applichem) plus 15.6 mM tris plus 30 mM ACES (Applichem) in the pH range of 5.7–10.0 were used. Both these mixtures also contained 120 mM NaCl (Sigma) and 100 μM dtpa (Sigma). The pH of the solutions was measured immediately after the reaction in all cases.

Expression and Purification of Proteins. Human WT PRDX5 (GenBank Accession No. NM_012094)³³ was expressed without its mitochondrial targeting sequence in *Escherichia coli* as a 6xHis-tagged protein and purified as previously described.¹² Mutants T44V and R127Q were generated by PCR-mediated site-directed mutagenesis using complementary primers containing base mismatch that converted the codon 44 for Thr to a codon for Val and the codon 127 for Arg to a codon for Gln, respectively. Numbering of codons and amino acids refers to mature human PRDX5.⁷ The mutants were cloned into pQE30 vector and expressed in the same way as WT PRDX5. Mismatched primers used were 5'-GCC TTC GTC CCG GGA TGT TCC A-3' (forward) and 5'-TCC CGG GAC GAA GGC CCC AGG-3' (reverse) for T44V mutant, and 5'-CGT CTT AAG CAG TTC TCC ATG G-3' (forward) and 5'-CCA TGG AGA ACT GCT TAA GAC-3' (reverse) for R127Q mutant.

Immediately before using, PRDX5 variants were reduced with 10 mM dithiothreitol for 30 min at neutral pH and room temperature. Excess dithiothreitol was removed using a HiTrap

desalting column (GE Healthcare) in an ÄKTAprime plus chromatography system (GE Healthcare); subsequently, protein concentration and thiol content were measured.

Determination of pK_a's. For measuring the pK_a of LMW thiolate we used the pH-dependent UV absorbance of the thiolate.³⁴ Thiol solutions were titrated in a buffer mixture containing acetic acid (5 mM), tris (2.6 mM), ethanolamine (2.6 mM), NaCl (145 mM), dtpa (100 μM), under argon. In a typical experiment, the thiol (final concentration 100–200 μM) was placed in the buffer (pH < 5), purged with argon for at least 30 min and titrated with small aliquots of 0.2 M NaOH (5 μL additions in a 4 mL spectrophotometer cuvette) with stirring. After each addition the equilibrium pH and UV spectrum from 220 to 350 nm were recorded using a 3 mm diameter glass electrode (Thermo Orion) and a Cary 50 spectrophotometer. Between 25 and 40 spectra were obtained in the range of pH from 5 to 13 for each compound. Either the absorbance at 240 nm or the maximum in the range 230–240 nm was plotted as a function of pH; the results were equal within experimental error. The absorbance vs pH plots were fitted to one of the following equations:

For simple thiols (2-mercaptoethanol, NAC, and captopril):

$$\text{Abs} = a \left(\frac{K_a}{K_a + [\text{H}^+]} \right) + c \quad (1)$$

where a is the absorbance of the thiolate, c is the background absorbance of the solution, and K_a is the ionization constant.

For DMSA, a dithiol:

$$\text{Abs} = \frac{a_1}{\frac{[\text{H}^+]}{K_{a1}} + 1} + \frac{a_2}{\frac{[\text{H}^+]^2}{K_{a1}K_{a2}} + \frac{[\text{H}^+]}{K_{a2}} + 1} + c \quad (2)$$

where a_1 and a_2 are the absorbance of the mono- and dithiolate, respectively, c is the background absorbance; K_{a1} and K_{a2} are the ionization constants.

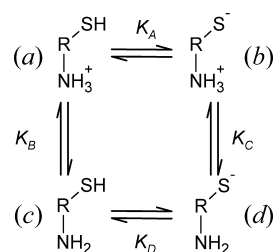
Finally, for aminothiols, (Cys, L-cysteine ethyl ester, GSH, L-cysteinyl-glycine and DL-homocysteine):

$$\text{Abs} = \frac{\text{Abs}_{\text{RS}^-} (K_A [\text{H}^+] + K_D K_B)}{[\text{H}^+]^2 + K_A [\text{H}^+] + K_D K_B} + c \quad (3)$$

where Abs_{RS^-} is the absorbance of the thiolate forms of the aminothiol (species b and d in Scheme 1), c is the background absorbance, and K_A , K_B , and K_D are the microscopic ionization constants according to Scheme 1.³⁴

Ionization constants of Cys residues in PRDX5 variants were measured through the pH-dependent variation of initial rate of reaction with mBBR as previously described.²⁹ Briefly, the initial slopes of fluorescence emission versus time at different pH values were fitted to a two pK_a function (eq 4).

Scheme 1. Microscopic Ionization Constants of an Aminothiol, according to Benesch³⁴



$$\text{slope} = \frac{a_1}{1 + \frac{K_{a1}}{[\text{H}^+]} + \frac{K_{a1}K_{a2}}{[\text{H}^+]^2}} + \frac{a_2}{\frac{[\text{H}^+]}{K_{a1}} + 1 + \frac{K_{a2}}{[\text{H}^+]}} + \frac{a_3}{\frac{[\text{H}^+]^2}{K_{a1}K_{a2}} + \frac{[\text{H}^+]}{K_{a2}} + 1} \quad (4)$$

where a_1 , a_2 , and a_3 are the pH-independent slopes of the reaction of the three acid–base species involved: diprotonated, monoprotated, and deprotonated, respectively. K_{a1} and K_{a2} are the ionization constants.

Rate Constants with mBBr. The nucleophilicity of LMW thiolates was measured as the pH-independent rate constant of their reaction with mBBr as previously described²⁹ for Cys, GSH, L-cysteine ethyl ester, NAC, 2-mercaptoethanol, captopril, and DMSA. Briefly, apparent second-order rate constants (k_{app}) were measured in the pH range from 6 to 12 under pseudo-first order conditions with thiol in excess at 25 °C. The values of k_{app} obtained were then plotted vs pH and fitted to a single ionization equation (eq 5) for simple thiols and to eq 6 in the case of aminothiols.

$$k_{\text{app}} = k_{\text{RS}^-} \left(\frac{K_a}{K_a + [\text{H}^+]} \right) \quad (5)$$

$$k_{\text{app}} = \frac{k_b \left(\frac{K_A}{K_B} \right) + k_d \left(\frac{K_D}{[\text{H}^+]} \right)}{\frac{K_A}{K_B} + \frac{K_D}{[\text{H}^+]} + \frac{[\text{H}^+]}{K_B}} + 1 \quad (6)$$

k_{RS^-} , k_b , and k_d are the pH-independent rate constants for the simple thiolate, the ammoniumthiolate, and the aminothiolate (species *b* and *d* in Scheme 1), respectively. The values of K_a , K_A , K_B , and K_D were those previously obtained by the UV-titration of the thiols.

Apparent second-order rate constants for PRDX5 reacting with mBBr were determined by the fluorescence of the product with excitation at 396 nm and emission at 475 nm. The reaction was carried out under pseudo-first order conditions with excess mBBr in tris-MES-acetate buffer at pH = 5.0 (TT44V) or 7.0 (R127Q) and 25 °C.

The pH-independent rate constants were calculated from the ratio between k_{app} and the normalized slope at the pH at which k_{app} was measured. This ratio was in turn used for each protein to extrapolate the pH-independent rate constants using the best fit parameters of eq 4, a_1 , a_2 , and a_3 , as previously described.²⁹

Rate Constants with Hydrogen Peroxide. The oxidation of LMW thiolates by H_2O_2 in tris-MES-acetate buffer, pH 7.06 \pm 0.04, was followed by the absorbance at 240 or 254 nm, under pseudo-first-order conditions with excess H_2O_2 , in a Varioskan Flash plate reader (Thermo) at 25 °C. Initial thiol concentrations were typically from 500 to 800 μM , whereas $[\text{H}_2\text{O}_2]_0$ ranged from 5 to 35 mM.

Oxidation of C47 of PRDX5 was monitored by the increase in intrinsic fluorescence as previously described⁸ under pseudo-first-order conditions with H_2O_2 in excess. WT PRDX5 was studied in an Applied Photophysics SX-20 stopped-flow spectrofluorimeter in tris-MES-acetate buffer pH 7.0 at 25 °C with $[\text{PRDX5}]_0 = 0.5 \mu\text{M}$ and $[\text{H}_2\text{O}_2]_0$ from 5 to 200 μM , with $\lambda_{\text{ex}} = 280 \text{ nm}$ and emission using a 320 nm filter. For T44V or R127Q PRDX5, a RX2000 Rapid Mixing Stopped-Flow with an Aminco-Bowman S2 spectrofluorimeter was used, with $\lambda_{\text{ex}} = 280 \text{ nm}$ and $\lambda_{\text{em}} = 333 \text{ nm}$. The ranges of $[\text{H}_2\text{O}_2]_0$ used were from 40 to 1000 μM for T44V and 0.73 to 8.9 mM for R127Q.

The change in fluorescence emission was followed for at least four half-lives and fitted to a first-order kinetic equation. The pseudo-first-order rate constants (k_{obs}) thus obtained were plotted vs $[\text{H}_2\text{O}_2]_0$ to obtain the apparent second-order rate constant (k_{app}).

Preparation of the Protein Template for Modeling.

The X-ray crystal structure of reduced WT PRDX5 complexed with benzoate was obtained from the Protein Data Bank (PDB ID: 1HD2¹²) and processed to be used as a template for the QM/MM models. After removal of benzoate and all crystallographic water molecules, hydrogen atoms were added by using the AMBER12 suite,³⁵ maintaining the expected ionization state for the amino acid residues at neutral pH, including C47 as thiolate. K^+ ions were added to achieve electroneutrality. Classical energy minimizations in aqueous solution were carried out by placing PRDX5 in a truncated octahedral box of TIP3P³⁶ water molecules maintaining a minimum distance of 12 Å between protein atoms and the box boundary. A 10 Å cutoff was applied for nonbonded interactions, and long-range electrostatic interactions were handled through periodic boundary conditions together with the Particle-mesh Ewald procedure,³⁷ with a charge grid spacing of 1 Å. Two minimization steps were run with the Amber ff99SB^{38,39} force field, first relaxing water molecules and ions for 2500 minimization steps (500 steepest descent, SD; 2000 conjugated gradient, CG), while the protein was kept frozen by applying a 500 kcal mol⁻¹ Å⁻² restraint. Once the environment was rearranged, the whole system was relaxed for 20000 minimization steps (5000 SD and 15000 CG). Finally, the stereochemical quality of protein structure in solution was verified through Ramachandran analysis, performed using PROCHECK.⁴⁰

QM/MM Models of Substrate Binding and Catalytic Mechanism.

QM/MM calculations were applied within the ONIOM formalism⁴¹ to characterize the initial complex (IC), the transition state (TS), and the final complex for H_2O_2 reduction by PRDX5. Substrate was manually introduced into the active site, taking as reference the positioning of H_2O_2 in the only available structure in which it appears bound to the active site of a peroxidase of *Aeropyrum pernix* K1 (PDB ID: 3A2V).⁴² A two-layer ONIOM(QM:MM) with mechanical embedding⁴³ was used as implemented in Gaussian 09⁴⁴ suite of programs. The QM region included 60 atoms belonging to substrate and conserved residues in the active site (T44, P45, G46, C47, and R127, see Figure 1) described by the B3LYP^{45,46}

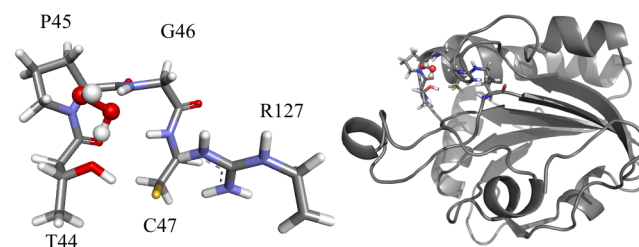


Figure 1. Molecular structure of PRDX5 in complex with H_2O_2 (2417 atoms). Left: detail of the QM region, including residues from the active site (sticks) and the H_2O_2 substrate (balls and sticks) in the oxygen track. Right: Location of the QM region in the protein, MM atoms (2357 atoms, 86 w/nuclear relaxation, cartoon) and QM atoms (60 atoms, sticks, colored by atom). The structure is based on PDB ID 1HD2 for the protein and 3A2V for the positioning of H_2O_2 , see details in Experimental and Computational Procedures.

density functional with an ultrafine pruned integration grid, and the 6-31+G(d,p)^{47,48} basis set. The rest of the protein (2357 atoms) was included in the MM region, represented by the AMBER parm96 force field.³⁹ Whereas H₂O₂ was parametrized using the General AMBER Force Field (GAFF)⁴⁹ and atomic charges obtained through the restrained electrostatic fit scheme (RESP),⁵⁰ the sulfenic acid formed at C47 was parametrized combining GAFF parameters and data from the literature.⁵¹

Partial geometry optimizations relaxing the position of 146 atoms including all the QM region plus residues in the MM classical region covalently bound to the former (F43, S48, K126, and F128) were conducted to find the structure of the stationary points. The rest of the protein was kept frozen along the calculations. The nature of each stationary point was verified through the analysis of the eigenvalues of the analytical Hessian matrix calculated at the same level. An intrinsic reaction coordinate (IRC)⁵² path was generated with the Euler Predictor-Corrector integrator⁵³ (80 points at each side of the reaction path, with an integration step size of 0.1 Bohr) to verify the connection of the TS to the initial and final complexes and gathering more information on the process. Once the structures of interest were characterized, partial charges for the QM atoms were refitted to get a more accurate description of electrostatics between QM and MM regions. A RESP⁵⁴ charge-refitting was thus applied, implying structural refinement through a new set of ONIOM optimizations. Finally, energetics was calculated at 298 K and 1 atm after harmonic normal mode vibrational analysis. Unscaled frequencies were used to calculate zero-point vibrational energy and thermal corrections to enthalpy, entropy contributions, and Gibbs free energies.

Descriptors of Nucleophilicity and Charge Reorganization along the Reaction Channel. To quantify the degree of charge reorganization and changes in strength of covalent and HB interactions induced by binding the substrate and the subsequent reaction, a natural population analysis (NPA) was performed based on natural bond orbitals (NBO).⁵⁵ NPA atomic charges⁵⁶ and Wiberg bond orders⁵⁷ were obtained through single-point PCM-B3LYP/6-31+G(d,p) calculations carried out on a collection of model structures of the active site (truncated ONIOM geometries at the QM region, capped with hydrogen atoms in bonds extending across the QM/MM boundary) taken from several points along the IRC's reactants channel. A dielectric constant $\epsilon = 35.7$ (the choice is rationalized in Figure S1, Supporting Information) and Bondi radii⁵⁸ were used to mimic with PCM the global electrostatic effects of the surrounding protein lacking in the QM model system after truncation. The energy of the HOMO KS orbital was extracted from ONIOM single-point calculations with electrostatic embedding (ONIOM-EE⁵⁹) on a set of complete structures taken from the ONIOM-ME IRC pathway. The HOMO KS corresponded to a nonbonding orbital on the thiolate, and its energy was analyzed as a predictor of the C_p nucleophilicity along the reaction path.

RESULTS

Rate Constants of LMW Thiolates. In order to have a consistent framework for comparing the reactivity of the C_p of PRDX5, we determined the rate constants of the reactions of LMW thiolates with mBBR and H₂O₂. As rate constants of nucleophilic substitution reactions depend on the pH distribution of the thiolate, we also determined the pK_a of the thiols studied under conditions consistent with our kinetic

experiments. A priori, the rate constants with H₂O₂ would provide a benchmark of thiolate reactivity in the absence of steric and protein-specific effects. The reaction with mBBR would allow a sensitive measurement of thiolate unspecific nucleophilicity using an alkylating agent not recognizable as a substrate for a peroxidase such as PRDX5.

Thiol pK_a's obtained by UV titration are summarized in Table 1 and compared to data obtained from the literature; the

Table 1. Thiol pK_a Values Obtained by UV Titration at 25 °C and 0.15 Ionic Strength^a

	pK _a	
	this work	literature value
simple thiols		
N-acetyl-L-cysteine	9.74 ± 0.01	9.55 ⁷⁸
2-mercaptoethanol	9.6 ± 0.01	9.61 ⁷⁹
captopril	10.1 ± 0.006	9.8 ⁸⁰
dithiols		
<i>meso</i> -2,3-dimercaptosuccinic acid	9.7 ± 0.03	9.68 ⁸¹
	11.3 ± 0.06	11.4 ⁸¹
aminothiols		
L-cysteine	8.29 ± 0.02	8.53 ³⁴
	9.67 ± 0.03	10.03 ³⁴
L-cysteine ethyl ester	7.5 ± 0.1	7.45 ³⁴
	9.0 ± 0.1	9.09 ³⁴
glutathione	8.94 ± 0.01	8.93 ⁸²
	9.27 ± 0.1	9.08 ⁸²
L-cysteinyl-glycine	7.95 ± 0.04	7.87 ³⁴
	9.28 ± 0.01	9.48 ³⁴
DL-homocysteine	9.1 ± 0.01	9.27 ⁷⁸
	9.98 ± 0.01	10.13 ⁷⁸

^aThe values listed correspond to pK_{a1} and pK_{a2} from eq 2 for DMSA, or pK_A and pK_D (eq 3) for aminothiols.

complete set of absorbance vs. pH plots and microscopic ionization constants are provided in the Supporting Information (Figure S2 and Table S1). Despite the differences in temperature and ionic strength used by other authors, the values are very similar in most cases.

The apparent rate constants of the reaction of LMW thiolates with mBBR are pH-dependent, as expected for a S_N2 reaction, and the pH profile can be fitted to a model considering microscopic pK_a's (eq 6) in the case of aminothiols, with the same pattern previously observed for cysteine.²⁹ The results for L-cysteine ethyl ester are shown as an example in Figure 2. Table 2 summarizes the values for pH-independent rate constants, which are used to construct the Bronsted correlation shown in Figure 3. The slope ($\beta = 0.52 \pm 0.08$), falls in the range of 0.2–0.52 determined for other S_N2 reactions of thiolates including redox^{8,60,61} and alkylation reactions.^{62,63}

The rate constants of LMW thiolates reacting with H₂O₂ follow a trend in which the pH-distribution of the thiolate is the most important factor contributing to k_{app} as observed in previous works.¹⁸ We chose to study the reaction at pH 7.0 in order to be at least two units below the second microscopic ionization constant of aminothiols (K_D) and therefore perform a simpler analysis considering only the reaction of the ammonium thiolate species, which is largely predominant at neutral pH. We decided to take this approach, instead of a more complex study involving the determination of pH-independent rate constants, since the ionization of H₂O₂ (pK_a = 11.18⁶⁴)

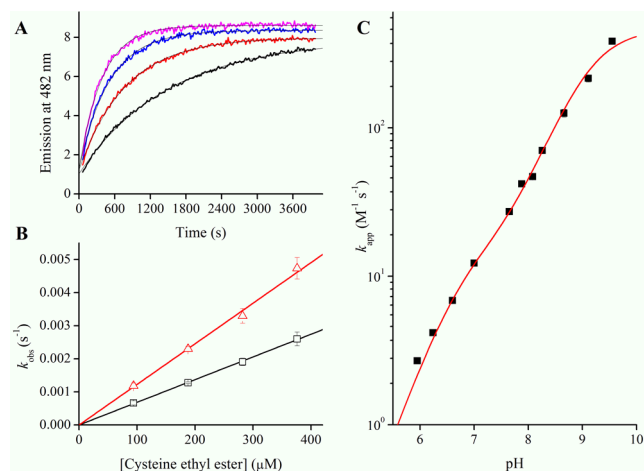


Figure 2. Reaction of L-cysteine ethyl ester with monobromobimane. (A) Time-courses of the reaction of 1 μM mBBR with (from bottom to top) 94, 188, 282, and 376 μM L-cysteine ethyl ester at pH 6.6. (B) Second-order plots at pH 6.6 (\square) and 7.0 (red open triangle) and 25 $^{\circ}\text{C}$. (C) pH profile of the apparent second-order rate constant (\blacksquare) fitted to eq 6 using $\text{p}K_{\text{A}} = 7.5$; $\text{p}K_{\text{B}} = 6.9$ and $\text{p}K_{\text{D}} = 9.0$ (continuous line). Best-fit parameters $k_{\text{b}} = 87 \pm 15$, $k_{\text{d}} = 460 \pm 20 \text{ M}^{-1} \text{ s}^{-1}$.

Table 2. pH-Independent Rate Constants of LMW Thiolsates with mBBR at 25 $^{\circ}\text{C}$ ^a

thiol	$k \text{ (M}^{-1} \text{ s}^{-1}\text{)}$
N-acetyl-L-cysteine	625 ± 25
2-mercaptoethanol	519 ± 31
captopril	1825 ± 29
meso-2,3-dimercaptosuccinic acid	1611 ± 84
L-cysteine	105 ± 1
	339 ± 72
L-cysteine ethyl ester	87 ± 15
	460 ± 20
glutathione	208 ± 32
	429 ± 29

^aFor L-cysteine, L-cysteine ethyl ester, and glutathione the two rate constants are k_{b} and k_{d} of eq 5, corresponding to the reaction of the ammoniumthiolate and the aminothiolate, respectively. For DMSA only the monothiolate rate constant was determined.

would interfere with thiols having $\text{p}K_{\text{a}}\text{'s} > 9$ further complicating the fitting of k_{app} vs pH profiles.

The values of k_{app} (Table 3) depend on $[\text{H}^+]$ according to eq 7, assuming that only one ionization equilibrium is relevant:

$$k_{\text{app}} = k \left(\frac{K_{\text{a}}}{K_{\text{a}} + [\text{H}^+]} \right) \quad (7)$$

Additionally, the pH-independent rate constant (k) of an $\text{S}_{\text{N}}2$ reaction is expected to follow a Brønsted relationship of the form:

$$\log k = \beta \text{p}K_{\text{a}} + C \quad (8)$$

Substituting eq 8 into eq 7 yields the Brønsted relationship for k_{app} as previously described:⁶⁰

$$\log k_{\text{app}} = \text{p}K_{\text{a}}(\beta - 1) + \log G - \log(K_{\text{a}} + [\text{H}^+]) \quad (9)$$

where β is the Brønsted nucleophilic factor and $\log G$ is the y-intercept of the Brønsted plot.

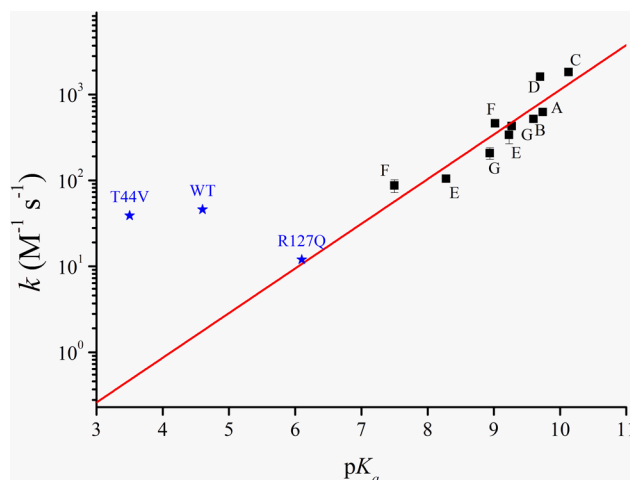


Figure 3. Brønsted plot for LMW thiolsates (\blacksquare) reacting with mBBR at 25 $^{\circ}\text{C}$. Linear fit parameters $k = 0.52 \text{ p}K_{\text{a}} - 2.1$. Reference for LMW thiolsates: A: NAC; B: 2-mercaptoethanol; C: captopril; D: DMSA; E: Cys; F: L-cysteine ethyl ester; G: GSH. PRDX5 pH-independent rate constants (blue star) are included for comparison and not included in the linear regression. See Discussion.

Table 3. Apparent Rate Constants of Thiols with H_2O_2 at pH 7.06 ± 0.04 , 25 $^{\circ}\text{C}$, and 0.15 Ionic Strength

thiol	$k_{\text{app}} \text{ (M}^{-1} \text{ s}^{-1}\text{)}$
N-acetyl-L-cysteine	0.082 ± 0.002
2-mercaptoethanol	0.07 ± 0.005
captopril	0.022 ± 0.002
meso-2,3-dimercaptosuccinic acid	0.009 ± 0.003
L-cysteine	0.84 ± 0.02
L-cysteine ethyl ester	1.40 ± 0.07
glutathione	0.42 ± 0.04
L-cysteinyl-glycine	1.54 ± 0.05
DL-homocysteine	0.18 ± 0.003

Fitting the k_{app} values in Table 3 to eq 9 yields the curve presented in Figure 4 with a β value of 0.27 ± 0.06 , which is also within the observed range for other $\text{S}_{\text{N}}2$ reactions (vide supra).

Reactivity of PRDX5 Variants. The pH profiles of the rate of alkylation of the PRDX5 variants with mBBR (Figure S3, Supporting Information) show two $\text{p}K_{\text{a}}\text{'s}$ similarly as we had previously observed for WT PRDX5.²⁹ The values of the $\text{p}K_{\text{a}}\text{'s}$ determined are presented in Table 4. It is apparent that the higher $\text{p}K_{\text{a}}$ remains essentially unchanged by mutations of T44 and R127, supporting the idea that it corresponds to the resolving cysteine, C151. On the other hand, the more acidic $\text{p}K_{\text{a}}$ is significantly affected by active-site mutations. A $\text{p}K_{\text{a}}$ of 5.2 was previously determined for C151S PRDX5 by the dependence of the rate constant of H_2O_2 reduction with pH, further identifying it with the $\text{p}K_{\text{a}}$ of C47.⁸ For WT PRDX5 the $\text{p}K_{\text{a}}$ of C47 was previously determined as 4.6.²⁹ As for the active-site mutants, R127Q has $\text{p}K_{\text{a}}$ of 6.1 ± 0.4 in line with the proposed stabilization of the thiolate by the cationic arginine, whereas we observed a drop of nearly one unit in the $\text{p}K_{\text{a}}$ value of C47 in T44V PRDX5 (3.5 ± 0.17).

The pH-independent rate constants of C47 with mBBR were obtained from the pH profile of the alkylation rate along with the single pH determination of k_{app} for PRDX5 (WT, T44V, and R127Q) as previously (Figure 5, Table 4).²⁹ We used these rate constants as a measure of the nonspecific nucleophilicity of

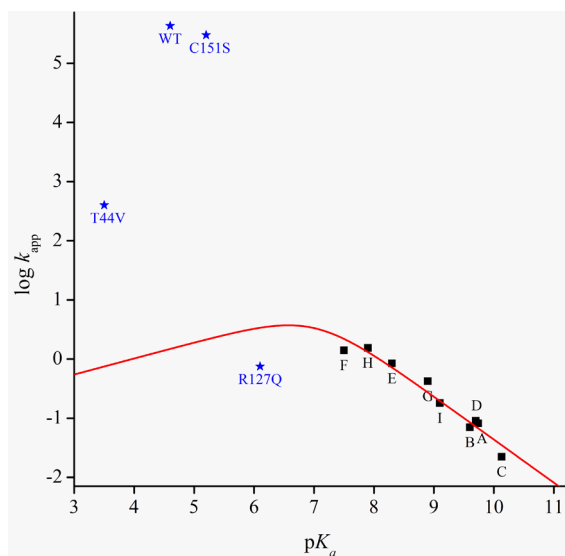


Figure 4. Brønsted plot of the apparent rate constants of LMW thioliates with H₂O₂ at pH 7.06 ± 0.04 and 25 °C. The values of k_{app} (■) were fitted to eq 9. Best-fit values $\beta = 0.27 \pm 0.06$, $\log G = -1.1 \pm 0.5$, continuous line. Reference for LMW thioliates. A: NAC; B: 2-mercaptoethanol; C: captopril; D: DMSA; E: Cys; F: L-cysteine ethyl ester; G: GSH; H: L-cysteinylglycine; I: DL-homocysteine. The values for PRDX5 variants (blue star) are included in the graph for comparison purposes, but were not considered for the fit.

the C47 thiolate. Placed in the context of the Brønsted relationship found for LMW thioliates (Figure 3), the nucleophilicity of WT and T44V PRDX5 appears above their expected values, whereas for the reaction with mBBr R127Q PRDX5 the rate constant falls exactly within the trend of LMW thioliates.

In the reaction of PRDX5 with H₂O₂ we found that T44V has a rate constant about 3 orders of magnitude smaller than the values for WT (Figure 6) and C151S.⁸ However, it is still 530 times faster than expected for a LMW thiolate, as can be seen in Figure 4. On the other hand, R127Q PRDX5 reacts extremely slowly, even below the value expected for a LMW thiolate. Thus, the rate constants of T44V and R127Q PRDX5 with H₂O₂ show a decrease relative to the enzymes with an intact active site (WT and C151S, Figure 4, Table 4) but each mutant is quantitatively different. Similar results had already been observed for tryparedoxin peroxidases^{21,65} and for peroxiredoxin Q,⁶⁶ in which the activity of mutants in active-site threonine and arginine is more than 2 orders of magnitude lower. The conserved arginine has also been shown to be critical for the rapid reduction of H₂O₂ by human peroxiredoxins 2 and 3⁶⁷ and probably, for the structuration of the active site.²¹ A very recent report⁶⁸ uses QM/MM calculations on human PRDX2 to study the thermodynamic

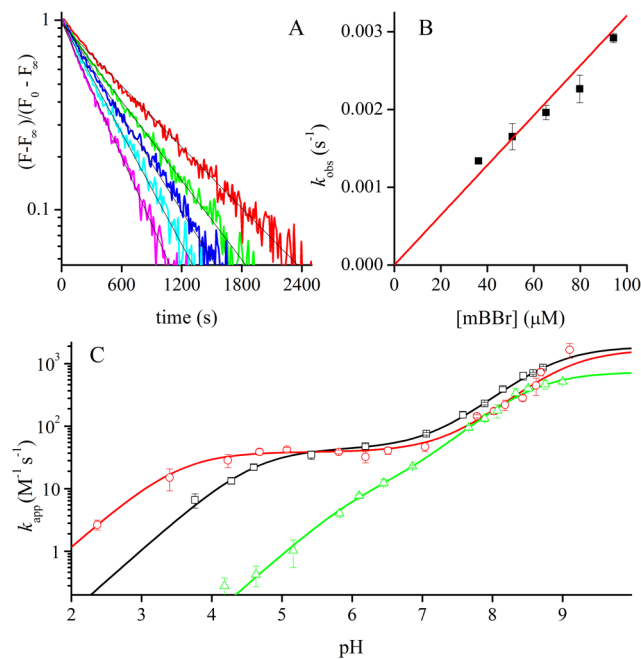


Figure 5. Rate constants of PRDX5 variants reacting with mBBr. (A) First-order plot of the fluorescence emission at 475 nm (F) upon reaction of 2.9 μM R127Q PRDX5 with (top to bottom) 36, 51, 65, 80, and 94 μM mBBr, pH = 7.0, 25 °C. (B) Second-order plot of the pseudo first-order rate constants vs initial concentration of mBBr. Slope of the linear regression 31 ± 1 M⁻¹ s⁻¹. (C) pH profile for the apparent rate constant, using the pH profile for the initial rate and the apparent rate constant at pH = 7.0 as previously described.²⁹ For WT (□), TT44V (red open circles) and R127Q (green open triangles) PRDX5, the data were fitted to eq 6 and yielded $k^{C47} = 46 \pm 2$, 39 ± 3 , and 12 ± 7 M⁻¹ s⁻¹, respectively.

stability of the sulfenic in the active site of WT and also in threonine and arginine mutants, and though they find significant differences, no mention is made to the effect of those differences on the kinetics of the process.

Structural Features in Substrate Binding and Catalysis by PRDX5. The ONIOM optimized structures of the key species in the peroxide reduction reaction are shown in Figure 7 including HB interactions confirmed through Wiberg bond-order analysis (Table S2, Supporting Information). The structure of the IC shows that H₂O₂ binds through HB to the active site. The peroxide HO group closer to C47 (O_R) serves as HB donor to the alcohol of T44 and as acceptor from the amide of G46. These interactions place the O_R at 4.2 Å from the thiolate. The involvement of hydrogen bonding between substrate and active site is consistent with the proposal of Hall et al.¹⁴ except that we did not find any structural evidence for a strong interaction between O_R and R127. Another important feature of the IC is that T44 serves as a HB

Table 4. pK_a and Rate Constants of PRDX5 Variants

PRDX5	pK _a		k(mBBr) (M ⁻¹ s ⁻¹)	k(H ₂ O ₂) (M ⁻¹ s ⁻¹)	
	C47	C151	pH-independent	apparent at (pH)	pH-independent
WT	4.6 ± 0.15 ^a	8.8 ± 0.19 ^a	46 ± 2 ^a	4.3 ± 0.1 × 10 ⁵ (7.1) ^b	4.3 × 10 ⁵
C151S	5.2 ± 0.2 ^b		ND	3.0 ± 0.5 × 10 ⁵ (7.4) ^c	3 × 10 ⁵
T44V	3.5 ± 0.17	9.0 ± 0.5	39 ± 3	4.0 ± 0.1 × 10 ² (6.9)	4 × 10 ²
R127Q	6.1 ± 0.4	8.5 ± 0.17	12 ± 7	0.65 ± 0.01 (6.9)	0.75

^aFrom ref 29. ^b3.0 × 10⁵ at pH 7.4 was previously reported, ref 8. ^cFrom ref 8.

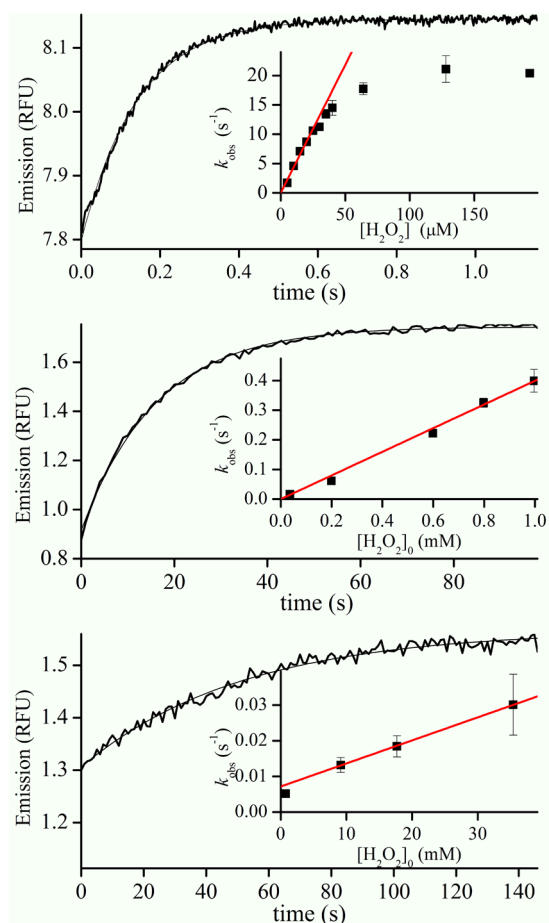


Figure 6. Oxidation of PRDX5 by H_2O_2 . Time-course of fluorescence increase upon oxidation of WT (top), T44V (middle) and R127Q (bottom) PRDX5 by 15 μM , 200 μM , and 17.7 mM H_2O_2 , respectively, at pH = 6.9 and 25 °C. The smooth lines correspond to the single exponential fits of the time courses. Insets: Second-order plots, slopes of the linear regressions $4.3 \pm 0.1 \times 10^5 \text{ M}^{-1} \text{ s}^{-1}$, $400 \pm 5 \text{ M}^{-1} \text{ s}^{-1}$, and $0.65 \pm 0.01 \text{ M}^{-1} \text{ s}^{-1}$. In the case of the WT PRDX5 the formation of the disulfide bond limits the value of k_{obs}^8 to a maximum of $21 \pm 0.1 \text{ s}^{-1}$ under our conditions, the linear fit only considers $[\text{H}_2\text{O}_2]_0 \leq 25 \mu\text{M}$.

donor to the C47 thiolate, which also receives two HB from the $^{\text{O}}\text{N}$ s of R127 and establishes a very weak interaction with the amide group of C47.

The TS shows a structure consistent with a $\text{S}_{\text{N}}2$ reaction in which the nucleophilic attack proceeds with an $\text{S}\cdots\text{O}\cdots\text{O}$ angle of 168° . In comparison with the IC, in the TS the distance from O_{R} to sulfur is shortened from 4.2 to 2.47 Å, and concurrently the $\text{O}_{\text{R}}\cdots\text{O}_{\text{L}}$ distance is lengthened from 1.4 to 1.75 Å. The approach of the O_{R} in the TS is accompanied by important changes in the HB network of the active site. Now, O_{R} receives HB from the amide of C47 and one $^{\text{O}}\text{NH}_2$ of R127 and still donates to the OH of T44. The amide of G46 has shifted and now donates to the leaving OH (O_{L}), consistent with the proposed oxygen track.¹⁴ Thus, the binding is reinforced through the formation of one additional HB. Additionally, the electric charge present in the thiolate in the IC (charge = -0.636 au) is partially transferred to O_{R} and O_{L} in the TS. The atomic NPA charge (Table S3, Supporting Information) on O_{R} decreases by 0.099 au and that on O_{L} also decreases by 0.211 au from IC to TS, making for a total charge transfer of -0.31 au and placing the overall anionic charge closer to the guanidinium

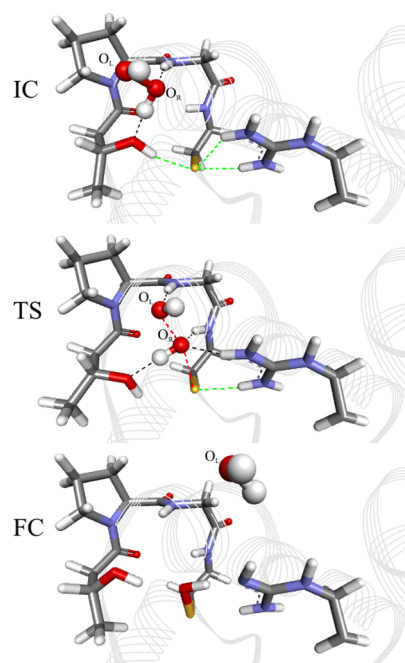


Figure 7. ONIOM optimized structures of the initial complex (IC), transition state (TS), and final complex (FC) of the reduction of H_2O_2 by PRDX5. The QM region is shown as sticks, and the rest of the protein (MM atoms) is shown as a flat ribbon. The HB network is shown as dotted lines, black for interactions involving H_2O_2 , and green for interactions involving C47 sulfur. Breaking/forming covalent bonds along the reaction coordinate are depicted as red dotted lines.

of R127. Both the additional HB of O_{R} and O_{L} and the charge redistribution contribute to the TS stabilization and accelerate the reaction. From the ONIOM(B3LYP/6-31+G(d,p): AMBER) level calculation a $\Delta G^{\ddagger,298}$ of 10.6 kcal/mol was obtained.

The HBs donated from T44 and R127 to the sulfur of C47 in the IC are greatly weakened in the TS. For instance, although the $\text{S}\cdots\text{O}(\text{T44})$ distance remains short (3.05 Å) the $\text{O}-\text{H}\cdots\text{S}$ angle is only 114.1° , quite far from an ideal HB geometry (Table S2, Supporting Information). Such a weakening of the HB would result in an increase of the cysteine nucleophilicity that will be discussed later. We have included an animation of the structural evolution along the IRC (Supporting Information Video SV1) in which it can be seen that the approaching O_{R} displaces the T44 and sequesters one of the $^{\text{O}}\text{NH}_2$ of R127 weakening their interaction with C47 causing the destabilization of the thiolate just before the TS.

After the TS two proton transfers occur sequentially (Table S4 and Figure S4, Supporting Information). First, O_{L} abstracts a proton from the newly formed sulfenic acid to form a water molecule that will eventually exit the active site. Second, the produced sulfenate receives a proton from the R127 guanidinium to restore the sulfenic acid. As a result, the final complex evidences not only the expected chemical transformation but also a major electrostatic rearrangement in the active site. From the thiolate-guanidinium ion-pair originally present, the reaction ends with a couple of hydrogen-bonded neutral moieties that could in turn facilitate the attack of the resolving thiolate to form the disulfide in the next reaction of the catalytic cycle.

DISCUSSION

For the two S_N2 reactions we studied, LMW thiolates have a behavior largely predictable by their Brønsted correlations. Our intention in including PRDX5 variants in Figures 3 and 4 was not to fit the protein behavior to the trend of LMW thiolates, but rather to underscore their differences and try to understand them in terms of reactivity, specificity and the detailed information on the mechanism provided by the QM/MM and QM (NPA/DFT) calculations.

The reaction with mBBr, seen in the light of Figure 3, shows that both WT and T44V PRDX5 are more nucleophilic than expected for their pK_a 's; R127Q, on the other hand, behaves just like a LMW thiolate. The increased nucleophilicity in the T44V mutant is consistent with our previous proposal that T44 restricts the nucleophilicity of C47 via hydrogen bonding.²² Although the rate constants are similar for WT and T44V, since T44V is more acidic the difference to the value expected for a LMW thiolate is larger for this mutant. Thus, the rate constant of T44V is 80 times higher than expected, whereas WT is only 25 times higher. In other words, the reaction with mBBr provides experimental evidence for the contribution of T44 to attenuate the nonspecific nucleophilicity of the thiolate. We expected a more pronounced difference, since in T44V there is at least one missing strong HB to the thiolate, but preliminary results from molecular dynamics simulations (not shown) indicate that the T44V mutation results in a more solvent-exposed C47 thiolate. Stabilizing interactions with water could lead to the lowered pK_a and moderate the observed increase in nucleophilicity.

Table 4 shows the rate constant for the reaction with H_2O_2 reacting with WT, T44V, and R127Q PRDX5 (obtained here) along with C151S PRDX5 (previously reported⁸). The rate constant of WT PRDX5, $4.3 \times 10^5 M^{-1} s^{-1}$, corresponds to a ΔG^\ddagger of 9.8 kcal/mol, in agreement with the value of 10.6 kcal/mol obtained by the QM/MM calculations. The WT protein reacts 5 orders of magnitude faster than expected for a LMW thiolate, which can be equated to a decrease in ΔG^\ddagger of approximately 7 kcal/mol, which is also in agreement with the experimental ΔG^\ddagger values of 15.9 and 16.9 kcal/mol measured for 2-mercaptoethanol⁶⁴ and cysteine,⁶⁹ respectively.

The rate constant of R127Q is four times lower than the value expected for a LMW thiolate in Figure 4. Taken together with the rate constant with mBBr, this behavior indicates that C47 in this mutant reacts pretty much like a LMW thiolate where the protein influences that favor catalysis are absent. We currently do not have structural evidence, but it would not be surprising that R127Q PRDX5 lacks a properly folded active site.

Also in Figure 4, T44V PRDX5 lies roughly halfway between WT and the expected value for a LMW thiolate represented by the continuous line, implying that a significant portion of the enhanced reactivity still occurs in the absence of T44. We had previously speculated that T44 may serve as a switch to C47 nucleophilicity²² by forming an HB in the resting enzyme but breaking it once the peroxide is positioned to react. Our QM/MM calculations are extremely revealing of the role of the active-site HB network along the reaction coordinate. In Figure 8 we have plotted the strength of the HB linked to C47 as Wiberg bond orders along with the energy of the HOMO KS, which corresponds to a nonbonding orbital on the thiolate, responsible for the nucleophilic attack. It can be seen that in the IC T44 and R127 form strong HB, while there is a weaker

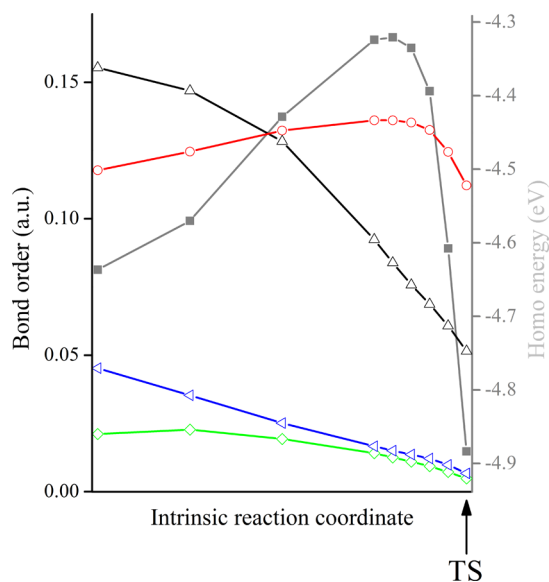


Figure 8. Bond order and HOMO energy evolution along the IRC. Wiberg bond order for the HBs donated to the thiolate of C47 from T44 (Δ) R127 (red open circles, blue open triangles) and C47 amide (green open diamonds) change along the IRC. Concurrently, the energy of the HOMO (gray solid boxes) has a maximum just before reaching the transition state and then stabilizes upon the nucleophilic attack in the TS. 1 eV = 23.06 kcal/mol.

interaction between the thiolate of C47 and its own amide group. On approaching the TS, the HB from T44 and one from R127 are significantly weakened; only one strong HB from R127 remains essentially constant throughout. The overall decrease in HB strength is reflected in the HOMO energy, which increases ca. 7.7 kcal/mol (0.334 eV) just before the transition state. In this respect, it can be interpreted that the HOMO stores the energy released by the breaking HBs upon H_2O_2 approach, and this energy is used to activate the nucleophilic thiolate; finally, the activated HOMO is stabilized by the formation of the covalent S–O bond in the TS.

The animation of the structure evolution along the IRC (Supporting Information SV1) shows that T44 acts as a pivot, guiding the movement of the O_R through a HB in which H_2O_2 acts as a donor. The same rotary movement of T44 along the $C\alpha$ – $C\beta$ bond that guides O_R on a collision course with C47 also disrupts the strong HB between T44 and the C47 thiolate observed in the initial complex. Therefore, T44 is involved in the enzyme specificity as it will interact and guide molecules able to act as HB donors, such as hydroperoxides and peroxyacids. T44 is also responsible for part of the kinetic proficiency of C47 because of the activating effect of the disruption of its HBs that prompt the thiolate for the nucleophilic attack. It is plausible then to ascribe the 3 orders of magnitude that separate T44V from WT in Figure 4 to this specific activation by T44.

Switching HB, Thiolate Destabilization, and TS Stabilization. The evolution of HB network along the reaction coordinate allows the assessment of the two proposed mechanisms for accelerating the reduction of H_2O_2 : thiolate destabilization and TS stabilization. As we saw in Figure 8, the C47 thiolate is destabilized concurrently with the approach of H_2O_2 because of weakened HB. Figure 9 shows that the sum of bond orders of all possible HB donors to C47 sulfur is halved in going from IC to TS. Additionally, the proposed stabilization of

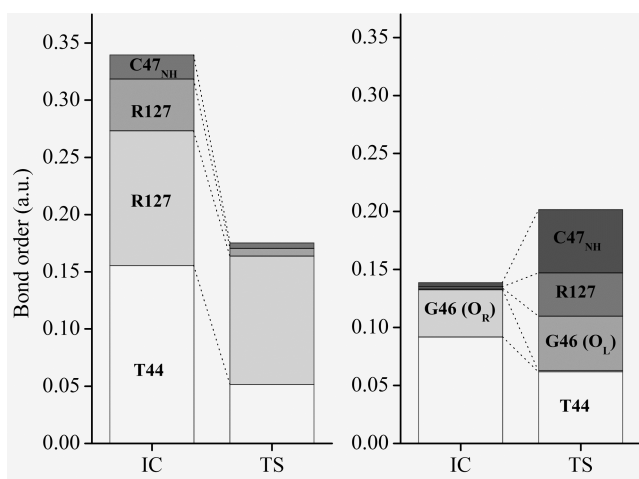


Figure 9. Differential strength of the interactions at the initial complex and TS stabilizing both C47 sulfur and H₂O₂. Left: C47 sulfur network, including HB from T44 and R127, an overall decrease by a factor of 2 is found. Right: H₂O₂ network, including HB from the oxygen track¹⁴ amides (G46 and C47) and to T44, a cumulative increase by a factor of 1.45 is found.

the TS¹⁴ is also apparent as the sum of interactions with H₂O₂, which an increase by a factor of 1.45 from IC to TS. Therefore, both the destabilization of the nucleophile and the stabilization of the TS are apparent from the evolution of the hydrogen bonds, and importantly, T44 participates in both, accelerating the reaction. Additionally, as mentioned before, the charge redistribution that places the anionic charge closer to the R127 guanidinium stabilizes the TS.

TS and Final Complex, Implications on Posterior Reactions of the Catalytic Cycle. In the TS, the nascent S–O bond order is 0.35 au, which is suggestively similar to the nucleophilic constant (β) determined in Figure 4. It has been proposed that the value of β corresponds to the degree of electron donation from the nucleophile in the transition state,⁷⁰ although other authors have disputed this assertion.⁷¹ Moreover, as previously mentioned, the total charge transfer from thiolate to H₂O₂ in the TS is -0.31 au, also consistent with the nucleophilic constant. In this work, the coincidence between β , bond order, and charge transfer in the TS is remarkable.

After the TS, the two proton transfers that occur may have important implications in the catalytic mechanism and in the subsequent reactions of the cycle. In the first place, the leaving hydroxide gains a proton from the sulfenic, producing the exit of water. Second, the sulfenate gets a proton from the R127 in a reaction that may appear unfavorable from the perspective of aqueous acid–base chemistry. The guanidinium from arginine is a very weak acid ($pK_a = 11.5^{72}$), whereas for sulfenic acid, pK_a 's of 6.1 and 6.6 have been determined for two other peroxidoxins.^{73,74} Therefore, the observed proton transfer would not take place in water spontaneously. However, media of lower dielectric constant and poorer anion-solvating capability than water exert a differential effect on neutral-acid dissociation (such as sulfenic) relative to cationic-acid dissociation (such as the arginine guanidinium group). For instance, acetic acid is stronger than triethylammonium in water (pK_a 's 4.6 and 10.3, respectively), whereas the opposite is true in acetonitrile ($\epsilon = 37.5$; pK_a 's 23.5 and 18.8, respectively).^{75,76} It is therefore to be expected that the polarizing sulfenate anion is capable of abstracting the proton from the guanidinium

group, thus neutralizing two electric charges and stabilizing both functional groups in the scarcely solvated environment of the active site of PRDX5.

Both proton transfers occur after the TS (Figure S4, Supporting Information) and therefore do not have any influence on the rate of reaction with H₂O₂. It may be surprising that no additional TS stabilization is gained through protonation of the leaving OH[−] (which is a strong base and thus a poor leaving group) in the TS. As further evidence for the absence of an acid catalysis effect in PRDX5, we have previously seen that the Brønsted plot of PRDX5 reacting with H₂O₂ and ONOOH, two peroxides differing in leaving-group pK_a , has roughly the same slope as the plots of GSH and bovine serum albumin reacting with the same peroxides.^{22,77}

Post-TS proton transfers may not influence the rate of reaction with H₂O₂ but may be very important for the subsequent steps in the catalytic cycle. The immediate reaction is the condensation of the sulfenic acid with the thiol of C151. The most favorable proton distribution for a such reaction would be having a thiolate in C151 (providing a good nucleophile) and the sulfenic acid in C47 (furnishing a better leaving group than sulfenate). C47 finishes the reduction of H₂O₂ as sulfenic and the deprotonated R127 may act as a base and abstract a proton from C151. This proton abstraction may be mediated by E143, a residue conserved in the PRDX5 subfamily and located roughly halfway between R127 and C151 (not shown). Actually, E143 and R127 lie along the 14 Å that separate the C47 sulfenic from C151 in the final complex. Finally, the redistribution of the charges in the active site after the reaction with H₂O₂ may trigger the conformational rearrangement needed to bring together C47 and C151.

Overall, our work has provided a framework to analyze the nucleophilicity and specificity of PRDX5 that can be extended to other protein thiols. In our case of study HB in the active site are crucial for two effects that make catalysis possible: the enhancement of thiolate nucleophilicity upon substrate entrance to the active site, and the stabilization of the transition state; in both effects T44 has a central role. The T44V mutant, with its thousand-fold decrease in the rate constant with the specific substrate H₂O₂, and its increased nucleophilicity toward the nonspecific electrophile mBBR reflects these phenomena. The two effects occur in a precise temporal sequence that ensures that the nucleophilicity of C47 becomes selectively available for substrates that bind to the active site through a HOOR functional group.

■ ASSOCIATED CONTENT

📄 Supporting Information

Figure S1. Rationale for choosing the dielectric constant. Figure S2. UV titration curves and fits for the thiols used in the article. Table S1. Microscopic ionization constants for the aminothiols studied. Figure S3. pH profiles of the initial slope of fluorescence increase for PRDX5 T44V and R127Q reacting with mBBR at 25 °C. Table S2. Wiberg bond orders for relevant pairs of atoms at the active site of PRDX5 and E_{HOMO} for points along the reaction coordinate. Table S3. NPA atomic charges for relevant atoms and functional groups at the active site of PRDX5 along the reaction coordinate. Table S4. Wiberg bond orders for proton acceptor/donor interactions at the active site of PRDX5. Figure S4. Evolution of the principal atomic pair distances involved in the heavy atom reorganization and proton transfer processes. Table S5. Coordinates for the optimized geometries of the IC, TS, and FC. Video SV1. An

animated sequence of the structure evolution along the reaction coordinate obtained from the QM/MM calculations. This material is available free of charge via the Internet at <http://pubs.acs.org>.

AUTHOR INFORMATION

Corresponding Author

*E-mail: gfe@fmed.edu.uy. Telephone/fax: 598 2525 0749.

Author Contributions

G.F.S. and E.L.C. designed research; S.P.L., F.S., M.V.T., B.A., A.C., B.K., and G.F.S. performed experimental research; S.P.L. and E.L.C. performed modeling research; G.F.S., S.P.L., and E.L.C. analyzed data; G.F.S., S.P.L., E.L.C., B.A., and B.M. wrote the article.

Funding

This work was supported by grants from CSIC, Universidad de la República, Uruguay (UdelaR), to F.S., B.A. and G.F.S.; Agencia Nacional de Investigación e Innovación (ANII), Uruguay, to S.P.L., E.L.C., and G.F.S. (INI-X-2010-2-2839 and FCE 5767); National Fund for Scientific Research (FRFC No. 2.4.603.09F) and the Fédération Wallonie-Bruxelles-Actions de Recherche Concertées (10/15-026) to B.K. S.P.L. is a recipient of a graduate scholarship from CAP, UdelaR. B.M. was partially supported by scholarships from ANII and CAP, UdelaR.

Notes

The authors declare no competing financial interest.

ACKNOWLEDGMENTS

We thank Dr. Rafael Radi for allowing the use of the SX-20 stopped-flow, and Mara Carreño and Lia Randall for their help with protein preparation.

ABBREVIATIONS

au, atomic units; CG, conjugated gradient; C_p, peroxidatic cysteine; C_R, resolving cysteine; DFT, density functional theory; DMSA, meso-2,3-dimercaptosuccinic acid; GSH, glutathione; HB, hydrogen bond; HOMO KS, highest occupied Kohn–Sham frontier orbital; IC, initial complex; IRC, intrinsic reaction coordinate; LMW, low molecular weight; mBB_r, monobromobimane; NAC, N-acetylcysteine; NPA, natural population analysis of the electron density; PRDX, peroxidase; QM/MM, quantum mechanics/molecular mechanics hybrid computational models; SD, steepest descent; TS, transition state; WT, wild type

REFERENCES

- (1) Richard, L. E., Peake, B. M., Rusak, S. A., Cooper, W. J., and Burritt, D. J. (2007) Production and decomposition dynamics of hydrogen peroxide in freshwater. *Environ. Chem.* 4, 49–54.
- (2) Knoops, B., Loumaye, E., and Van Der Eecken, V. (2007) Evolution of the peroxidases. *Subcell. Biochem.* 44, 27–40.
- (3) Kim, I. H., Kim, K., and Rhee, S. G. (1989) Induction of an antioxidant protein of *Saccharomyces cerevisiae* by O₂, Fe³⁺, or 2-mercaptoethanol. *Proc. Natl. Acad. Sci. U. S. A.* 86, 6018–6022.
- (4) Tavender, T. J., Springate, J. J., and Bulleid, N. J. (2010) Recycling of peroxidase IV provides a novel pathway for disulphide formation in the endoplasmic reticulum. *EMBO J.* 29, 4185–4197.
- (5) Fomenko, D. E., Koc, A., Agisheva, N., Jacobsen, M., Kaya, A., Malinowski, M., Rutherford, J. C., Siu, K. L., Jin, D. Y., Winge, D. R., and Gladyshev, V. N. (2011) Thiol peroxidases mediate specific genome-wide regulation of gene expression in response to hydrogen peroxide. *Proc. Natl. Acad. Sci. U. S. A.* 108, 2729–2734.

- (6) Reeves, S. A., Parsonage, D., Nelson, K. J., and Poole, L. B. (2012) Kinetic and thermodynamic features reveal that *Escherichia coli* BCP is an unusually versatile peroxidase. *Biochemistry* 50, 8970–8981.

- (7) Manta, B., Hugo, M., Ortiz, C., Ferrer-Sueta, G., Trujillo, M., and Denicola, A. (2009) The peroxidase and peroxynitrite reductase activity of human erythrocyte peroxidase 2. *Arch. Biochem. Biophys.* 484, 146–154.

- (8) Trujillo, M., Clippe, A., Manta, B., Ferrer-Sueta, G., Smeets, A., Declercq, J. P., Knoops, B., and Radi, R. (2007) Pre-steady state kinetic characterization of human peroxidase 5: taking advantage of Trp84 fluorescence increase upon oxidation. *Arch. Biochem. Biophys.* 467, 95–106.

- (9) Reyes, A. M., Hugo, M., Trostchansky, A., Capece, L., Radi, R., and Trujillo, M. (2011) Oxidizing substrate specificity of *Mycobacterium tuberculosis* alkyl hydroperoxide reductase E: kinetics and mechanisms of oxidation and overoxidation. *Free. Radic. Biol. Med.* 51, 464–473.

- (10) Peskin, A. V., Low, F. M., Paton, L. N., Maghzal, G. J., Hampton, M. B., and Winterbourn, C. C. (2007) The high reactivity of peroxidase 2 with H₂O₂ is not reflected in its reaction with other oxidants and thiol reagents. *J. Biol. Chem.* 282, 11885–11892.

- (11) Wood, Z. A., Schröder, E., Robin Harris, J., and Poole, L. B. (2003) Structure, mechanism and regulation of peroxidases. *Trends Biochem. Sci.* 28, 32–40.

- (12) Declercq, J. P., Evrard, C., Clippe, A., Stricht, D. V., Bernard, A., and Knoops, B. (2001) Crystal structure of human peroxidase 5, a novel type of mammalian peroxidase at 1.5 Å resolution. *J. Mol. Biol.* 311, 751–759.

- (13) Evrard, C., Capron, A., Marchand, C., Clippe, A., Wattiez, R., Soumillion, P., Knoops, B., and Declercq, J. P. (2004) Crystal structure of a dimeric oxidized form of human peroxidase 5. *J. Mol. Biol.* 337, 1079–1090.

- (14) Hall, A., Parsonage, D., Poole, L. B., and Karplus, P. A. (2010) Structural evidence that peroxidase catalytic power is based on transition-state stabilization. *J. Mol. Biol.* 402, 194–209.

- (15) Smeets, A., Marchand, C., Linard, D., Knoops, B., and Declercq, J. P. (2008) The crystal structures of oxidized forms of human peroxidase 5 with an intramolecular disulfide bond confirm the proposed enzymatic mechanism for atypical 2-Cys peroxidases. *Arch. Biochem. Biophys.* 477, 98–104.

- (16) Dubuisson, M., Vander Stricht, D., Clippe, A., Etienne, F., Nausier, T., Kissner, R., Koppenol, W. H., Rees, J. F., and Knoops, B. (2004) Human peroxidase 5 is a peroxynitrite reductase. *FEBS Lett.* 571, 161–165.

- (17) Jencks, W. P. (1975) Binding energy, specificity, and enzymic catalysis: the circe effect. *Adv. Enzymol. Relat. Areas Mol. Biol.* 43, 219–410.

- (18) Winterbourn, C. C., and Metodiewa, D. (1999) Reactivity of biologically important thiol compounds with superoxide and hydrogen peroxide. *Free. Radic. Biol. Med.* 27, 322–328.

- (19) Singh, R., and Whitesides, G. M. (1990) Comparisons of rate constants for thiolate-disulfide interchange in water and in polar aprotic-solvents using dynamic H-1-NMR line-shape analysis. *J. Am. Chem. Soc.* 112, 1190–1197.

- (20) Smith, J. N., Hoffman, J. T., Shirin, Z., and Carrano, C. J. (2005) H-bonding interactions and control of thiolate nucleophilicity and specificity in model complexes of zinc metalloproteins. *Inorg. Chem.* 44, 2012–2017.

- (21) Flohé, L., Budde, H., Bruns, K., Castro, H., Clos, J., Hofmann, B., Kansal-Kalavar, S., Krumme, D., Menge, U., Plank-Schumacher, K., Sztajer, H., Wissing, J., Wylegalla, C., and Hecht, H. J. (2002) Tryparedoxin peroxidase of *Leishmania donovani*: molecular cloning, heterologous expression, specificity, and catalytic mechanism. *Arch. Biochem. Biophys.* 397, 324–335.

- (22) Ferrer-Sueta, G., Manta, B., Botti, H., Radi, R., Trujillo, M., and Denicola, A. (2011) Factors affecting protein thiol reactivity and specificity in peroxide reduction. *Chem. Res. Toxicol.* 24, 434–450.

- (23) Forman, H. J., Ursini, F., and Maiorino, M. (2014) An overview of mechanisms of redox signaling. *J. Mol. Cell Cardiol.* 73, 2–9.
- (24) Randall, L. M., Ferrer-Sueta, G., and Denicola, A. (2013) Peroxiredoxins as preferential targets in H₂O₂-induced signaling. *Methods Enzymol.* 527, 41–63.
- (25) Leere Øiestad, Å. M., Petersen, A. C., Bakken, V., Vedde, J., and Uggerud, E. (2001) The oxidative power of protonated hydrogen peroxide. *Angew. Chem., Int. Ed.* 40, 1305–1309.
- (26) Leere Øiestad, E., Harvey, J. N., and Uggerud, E. (2000) Unimolecular reactions of protonated hydrogen peroxide: A quantum chemical survey. *J. Phys. Chem. A* 104, 8382–8388.
- (27) Olah, G. A., Yoneda, N., and Parker, D. G. (1977) Oxyfunctionalization of hydrocarbons. 4. Fluorosulfuric acid-antimony pentafluoride, fluorosulfuric acid, sulfuric acid, and hydrofluoric acid induced electrophilic oxygenation of alkanes with hydrogen peroxide. *J. Am. Chem. Soc.* 99, 483–488.
- (28) Grasseti, D. R., and Murray, J. F., Jr. (1967) Determination of sulfhydryl groups with 2,2'- or 4,4'-dithiodipyridine. *Arch. Biochem. Biophys.* 119, 41–49.
- (29) Sardi, F., Manta, B., Portillo-Ledesma, S., Knoops, B., Comini, M. A., and Ferrer-Sueta, G. (2013) Determination of acidity and nucleophilicity in thiols by reaction with monobromobimane and fluorescence detection. *Anal. Biochem.* 435, 74–82.
- (30) Kosower, E. M., and Kosower, N. S. (1995) Bromobimane probes for thiols. *Methods Enzymol.* 251, 133–148.
- (31) Claiborne, A. (1985) Catalase Activity, in *Handbook of Methods for Oxygen Radical Research* (Greenwald, R. A., Ed.), pp 283–284, CRC Press, Boca Raton, FL.
- (32) Ellis, K. J., and Morrison, J. F. (1982) Buffers of constant ionic strength for studying pH-dependent processes. *Methods Enzymol.* 87, 405–426.
- (33) Knoops, B., Clippe, A., Bogard, C., Arsalane, K., Wattiez, R., Hermans, C., Duconseille, E., Falmagne, P., and Bernard, A. (1999) Cloning and characterization of AOEB166, a novel mammalian antioxidant enzyme of the peroxiredoxin family. *J. Biol. Chem.* 274, 30451–30458.
- (34) Benesch, R. E., and Benesch, R. (1955) The acid strength of the -SH group in cysteine and related compounds. *J. Am. Chem. Soc.* 77, 5877–5881.
- (35) Case, D. A., Darden, T. A., Cheatham, T. E., III, Simmerling, C. L., Wang, J., Duke, R. E., Luo, R., Walker, R. C., Zhang, W., Merz, K. M., Roberts, B., Hayik, S., Roitberg, A., Seabra, G., Swails, J., Goetz, A. W., Kolossváry, I., Wong, K. F., Paesani, F., Vanicek, J., Wolf, R. M., Liu, J., Wu, X., Brozell, S. R., Steinbrecher, T., Gohlke, H., Cai, Q., Ye, X., Wang, J., Hsieh, M.-J., Cui, G., Roe, D. R., Mathews, D. H., Seetin, M. G., Salomon-Ferrer, R., Sagui, C., Babin, V., Luchko, T., Gusarov, S., Kovalenko, A., and Kollman, P. A. (2012) *AMBER 12 suite*, University of California, San Francisco.
- (36) Jorgensen, W. L., Chandrasekhar, J., Madura, J. D., Impey, R. W., and Klein, M. L. (1983) Comparison of Simple Potential Functions for Simulating Liquid Water. *J. Chem. Phys.* 79, 926–935.
- (37) Toukmaji, A., Sagui, C., Board, J., and Darden, T. (2000) Efficient particle-mesh Ewald based approach to fixed and induced dipolar interactions. *J. Chem. Phys.* 113, 10913–10927.
- (38) Wang, J., Cieplak, P., and Kollman, P. (2000) How well does a restrained electrostatic potential (RESP) model perform in calculating conformational energies of organic and biological molecules? *J. Comput. Chem.* 21, 1049–1074.
- (39) Cornell, W. D., Cieplak, P., Bayly, C. I., Gould, I. R., Merz, K. M., Jr., Ferguson, D. M., Spellmeyer, D. C., Fox, T., Caldwell, J. W., and Kollman, P. A. (1995) A second generation force-field for the simulation of proteins, nucleic-acids, and organic-molecules. *J. Am. Chem. Soc.* 117, 5179–5197.
- (40) Laskowski, R. A., MacArthur, M. W., Moss, D. S., and Thornton, J. M. (1993) PROCHECK: a program to check the stereochemical quality of protein structures. *J. Appl. Crystallogr.* 26, 283–291.
- (41) Svensson, M. H. S., Froese, R. D. J., Matsubara, T., Sieber, S., and Morokuma, K. (1996) ONIOM: A multilayered integrated MO+MM method for geometry optimization and single point energy predictions. A test for Diels-Alder reactions and Pt(P(t-Bu)₃)₂ + H₂ oxidative addition. *J. Phys. Chem.* 100, 19357–19363.
- (42) Nakamura, T., Kado, Y., Yamaguchi, T., Matsumura, H., Ishikawa, K., and Inoue, T. (2010) Crystal structure of peroxiredoxin from *Aeropyrum pernix* K1 complexed with its substrate, hydrogen peroxide. *J. Biochem.* 147, 109–115.
- (43) Bakowies, D., and Thiel, W. (1996) Hybrid Models for Combined Quantum Mechanical and Molecular Mechanical Approaches. *J. Phys. Chem.* 100, 10580–10594.
- (44) Frisch, M. J., Trucks, G. W., Schlegel, H. B., Scuseria, G. E., Robb, M. A., Cheeseman, J. R., Scalmani, G., Barone, V., Mennucci, B., Petersson, G. A., Nakatsuji, H., Caricato, M., Li, X., Hratchian, H. P., Izmaylov, A. F., Bloino, J., Zheng, G., Sonnenberg, J. L., Hada, M., Ehara, M., Toyota, K., Fukuda, R., Hasegawa, J., Ishida, M., Nakajima, T., Honda, Y., Kitao, O., Nakai, H., Vreven, T., Montgomery Jr., J. A., Peralta, J. E., Ogliaro, F., Bearpark, M. J., Heyd, J., Brothers, E. N., Kudin, K. N., Staroverov, V. N., Kobayashi, R., Normand, J., Raghavachari, K., Rendell, A. P., Burant, J. C., Iyengar, S. S., Tomasi, J., Cossi, M., Rega, N., Millam, N. J., Klene, M., Knox, J. E., Cross, J. B., Bakken, V., Adamo, C., Jaramillo, J., Gomperts, R., Stratmann, R. E., Yazyev, O., Austin, A. J., Cammi, R., Pomelli, C., Ochterski, J. W., Martin, R. L., Morokuma, K., Zakrzewski, V. G., Voth, G. A., Salvador, P., Dannenberg, J. J., Dapprich, S., Daniels, A. D., Farkas, Ö., Foresman, J. B., Ortiz, J. V., Cioslowski, J., and Fox, D. J. (2009) *Gaussian 09*, Gaussian, Inc., Wallingford, CT, USA.
- (45) Becke, A. D. (1993) A new mixing of Hartree-Fock and local density-functional theories. *J. Chem. Phys.* 98, 1372–1377.
- (46) Lee, C. L., Yang, W., and Parr, R. G. (1988) Development of the Colle-Salvetti correlation energy formula into a functional of the electron density. *Phys. Rev. B* 37, 785–789.
- (47) Hehre, W. L., Ditchfield, R., and Pople, J. A. (1972) Self-consistent molecular orbital methods. XII. Further extensions of Gaussian-type basis sets for use in molecular orbital studies of organic molecules. *J. Chem. Phys.* 56, 2257–2261.
- (48) Clark, T., Chandrasekhar, J., and Schleyer, P. V. R. (1983) Efficient diffuse function-augmented basis sets for anion calculations. III. The 3-21+G basis set for first-row elements Li–F. *J. Comput. Chem.* 4, 294–201.
- (49) Wang, J., Wolf, R. M., Caldwell, J. W., Kollman, P. A., and Case, D. A. (2004) Development and Testing of a General Amber Force Field. *J. Comput. Chem.* 25, 1157–1173.
- (50) Bayly, C. I., Cieplak, P., Cornell, W. D., and Kollman, P. A. (1993) A Well-Behaved Electrostatic Potential Based Method Using Charge Restraints for Deriving Atomic Charges: The RESP Model. *J. Phys. Chem.* 10269–10280.
- (51) Kona, J., and Brinck, T. (2006) A combined molecular dynamics simulation and quantum chemical study on the mechanism for activation of the OxyR transcription factor by hydrogen peroxide. *Org. Biomol. Chem.* 4, 3468–3478.
- (52) Fukui, K. (1981) The path of chemical-reactions - The IRC approach. *Acc. Chem. Res.* 14, 363–368.
- (53) Hratchian, H. P., Frisch, M. J., and Schlegel, H. B. (2010) Steepest descent reaction path integration using a first-order predictor-corrector method. *J. Chem. Phys.* 133, 224101–224108.
- (54) Breneman, C. M., and Wiberg, K. B. (1990) Determining atom-centered monopoles from molecular electrostatic potentials—the need for high sampling density in formamide conformational-analysis. *J. Comput. Chem.* 11, 361–373.
- (55) Glendening, E. D., Landis, C. R., and Weinhold, F. (2012) Natural bond orbital methods. *WIREs Comput. Mol. Sci.* 2, 1–42.
- (56) Reed, A. E., Weinstock, R. B., and Weinhold, F. (1985) Natural population analysis. *J. Chem. Phys.* 83, 735–746.
- (57) Wiberg, K. B. (1968) Application of the Pople-Santry-Segal CNDO method to the cyclopropylcarbinyl and cyclobutyl cation and to bicyclobutane. *Tetrahedron* 24, 1083–1096.
- (58) Bondi, A. (1964) van der Waals volume and radii. *J. Phys. Chem.* 68, 441–451.
- (59) Vreven, T., Byun, K. S., Komáromi, I., Dapprich, S., Montgomery, J. A., Morokuma, K., and Frisch, M. J. (2006)

Combining Quantum Mechanics Methods with Molecular Mechanics Methods in ONIOM. *J. Chem. Theory Comput.* 2, 815–826.

(60) Roberts, D. D., Lewis, S. D., Ballou, D. P., Olson, S. T., and Shafer, J. A. (1986) Reactivity of small thiolate anions and cysteine-25 in papain toward methyl methanethiosulfonate. *Biochemistry* 25, 5595–5601.

(61) Wilson, J. M., Bayer, R. J., and Hupe, D. J. (1977) Structure-reactivity correlations for the thiol-disulfide interchange reaction. *J. Am. Chem. Soc.* 99, 7922–7926.

(62) Bednar, R. A. (1990) Reactivity and pH dependence of thiol conjugation to N-ethylmaleimide: detection of a conformational change in chalcone isomerase. *Biochemistry* 29, 3684–3690.

(63) Reuben, D. M. E., and Bruce, T. C. (1976) Reaction of thiol anions with benzene oxide and malachite green. *J. Am. Chem. Soc.* 98, 114–121.

(64) Leung, P. S. K., and Hoffmann, M. R. (1985) Kinetics and mechanism of the oxidation of 2-mercaptoethanol by hydrogen peroxide in aqueous solution. *J. Phys. Chem.* 89, 5267–5271.

(65) Montemartini, M., Kalisz, H. M., Hecht, H. J., Steinert, P., and Flohe, L. (1999) Activation of active-site cysteine residues in the peroxiredoxin-type tryparedoxin peroxidase of *Crithidia fasciculata*. *Eur. J. Biochem.* 264, 516–524.

(66) Lamkemeyer, P., Laxa, M., Collin, V., Li, W., Finkemeier, I., Schottler, M. A., Holtkamp, V., Tognetti, V. B., Issakidis-Bourguet, E., Kandlbinder, A., Weis, E., Miginiac-Maslow, M., and Dietz, K. J. (2006) Peroxiredoxin Q of *Arabidopsis thaliana* is attached to the thylakoids and functions in context of photosynthesis. *Plant J.* 45, 968–981.

(67) Nagy, P., Karton, A., Betz, A., Peskin, A. V., Pace, P., O'Reilly, R. J., Hampton, M. B., Radom, L., and Winterbourn, C. C. (2011) Model for the exceptional reactivity of peroxiredoxins 2 and 3 with hydrogen peroxide: a kinetic and computational study. *J. Biol. Chem.* 286, 18048–18055.

(68) Olah, J., van Bergen, L., De Proft, F., and Roos, G. (2014) How does the protein environment optimize the thermodynamics of thiol sulfenylation? Insights from model systems to QM/MM calculations on human 2-Cys peroxiredoxin. *J. Biomol. Struct. Dyn.*, 1–13.

(69) Luo, D., Smith, S. W., and Anderson, B. D. (2005) Kinetics and mechanism of the reaction of cysteine and hydrogen peroxide in aqueous solution. *J. Pharm. Sci.* 94, 304–316.

(70) Bulaj, G., Kortemme, T., and Goldenberg, D. P. (1998) Ionization-reactivity relationships for cysteine thiols in polypeptides. *Biochemistry* 37, 8965–8972.

(71) Szajewski, R. P., and Whitesides, G. M. (1980) Rate constants and equilibrium constants for thiol-disulfide interchange reactions involving oxidized glutathione. *J. Am. Chem. Soc.* 102, 2011–2026.

(72) Clarke, E. R., and Martell, A. E. (1970) Metal chelates of arginine and related ligands. *J. Inorg. Nucl. Chem.* 32, 911–926.

(73) Poole, L. B., and Ellis, H. R. (2002) Identification of cysteine sulfenic acid in AhpC of alkyl hydroperoxide reductase. *Methods Enzymol.* 348, 122–136.

(74) Hugo, M., Turell, L., Manta, B., Botti, H., Monteiro, G., Netto, L. E., Alvarez, B., Radi, R., and Trujillo, M. (2009) Thiol and sulfenic acid oxidation of AhpE, the one-cysteine peroxiredoxin from *Mycobacterium tuberculosis*: kinetics, acidity constants, and conformational dynamics. *Biochemistry* 48, 9416–9426.

(75) Kaljurand, I., Kütt, A., Sooväli, L., Rodima, T., Mäemets, V., Leito, I., and Koppel, I. A. (2005) Extension of the self-consistent spectrophotometric basicity scale in acetonitrile to a full span of 28 pK_a units: unification of different basicity scales. *J. Org. Chem.* 70, 1019–1028.

(76) Kütt, A., Leito, I., Kaljurand, I., Sooväli, L., Vlasov, V. M., Yagupolskii, L. M., and Koppel, I. A. (2006) A comprehensive self-consistent spectrophotometric acidity scale of neutral Brønsted acids in acetonitrile. *J. Org. Chem.* 71, 2829–2838.

(77) Trindade, D. F., Cerchiaro, G., and Augusto, O. (2006) A role for peroxymonocarbonate in the stimulation of biothiols peroxidation by the bicarbonate/carbon dioxide pair. *Chem. Res. Toxicol.* 19, 1475–1482.

(78) Connett, P. H., and Wetterhahn, K. E. (1986) Reaction of chromium(VI) with thiols: pH dependence of chromium(VI) thio ester formation. *J. Am. Chem. Soc.* 108, 1842–1847.

(79) Jencks, W. P., and Salvesen, K. (1971) Equilibrium deuterium isotope effects on the ionization of thiol acids. *J. Am. Chem. Soc.* 93, 4433–4436.

(80) Rabenstein, D. L., and Isab, A. A. (1982) Conformational and acid-base equilibria of captopril in aqueous solution. *Anal. Chem.* 54, 526–529.

(81) Aposhian, H. V., and Aposhian, M. M. (1990) meso-2,3-Dimercaptosuccinic acid: chemical, pharmacological and toxicological properties of an orally effective metal chelating agent. *Annu. Rev. Pharmacol. Toxicol.* 30, 279–306.

(82) Rabenstein, D. L. (1973) Nuclear magnetic resonance studies of the acid-base chemistry of amino acids and peptides. I. Microscopic ionization constants of glutathione and methylmercury-complexed glutathione. *J. Am. Chem. Soc.* 95, 2797–2803.